

## CLINICAL SCIENCE

# A proton nuclear magnetic resonance-based metabonomics study of metabolic profiling in immunoglobulin a nephropathy

Weiguo Sui,<sup>1</sup> Liping Li,<sup>1,II</sup> Wenti Che,<sup>1</sup> Guimai Zuo,<sup>1</sup> Jiejing Chen,<sup>1</sup> Wuxian Li,<sup>III</sup> Yong Dai<sup>I,IV</sup>

<sup>1</sup>181<sup>st</sup> Hospital Guangxi, Central Laboratory, Laboratory of Metabolic Diseases Research, Guangxi Province, China. <sup>II</sup>Guangxi Normal University, the Life Science College, Guangxi Province, China. <sup>III</sup>Key Laboratory of Laboratory Medical Diagnostics of Education Ministry, Chongqing Medical University, Chongqing, China. <sup>IV</sup>Clinical Medical Research Center, the Second Clinical Medical College of Jinan University (Shenzhen People's Hospital), Shenzhen, Guangdong Province, China.

**OBJECTIVES:** Immunoglobulin A nephropathy is the most common cause of chronic renal failure among primary glomerulonephritis patients. The ability to diagnose immunoglobulin A nephropathy remains poor. However, renal biopsy is an inconvenient, invasive, and painful examination, and no reliable biomarkers have been developed for use in routine patient evaluations. The aims of the present study were to identify immunoglobulin A nephropathy patients, to identify useful biomarkers of immunoglobulin A nephropathy and to establish a human immunoglobulin A nephropathy metabolic profile.

**METHODS:** Serum samples were collected from immunoglobulin A nephropathy patients who were not using immunosuppressants. A pilot study was undertaken to determine disease-specific metabolite biomarker profiles in three groups: healthy controls (N = 23), low-risk patients in whom immunoglobulin A nephropathy was confirmed as grades I-II by renal biopsy (N = 23), and high-risk patients with nephropathies of grades IV-V (N = 12). Serum samples were analyzed using proton nuclear magnetic resonance spectroscopy and by applying multivariate pattern recognition analysis for disease classification.

**RESULTS:** Compared with the healthy controls, both the low-risk and high-risk patients had higher levels of phenylalanine, *myo*-Inositol, lactate, L6 lipids (= CH-CH<sub>2</sub>-CH = O), L5 lipids (-CH<sub>2</sub>-C = O), and L3 lipids (-CH<sub>2</sub>-CH<sub>2</sub>-C = O) as well as lower levels of β-glucose, α-glucose, valine, tyrosine, phosphocholine, lysine, isoleucine, glycerolphosphocholine, glycine, glutamine, glutamate, alanine, acetate, 3-hydroxybutyrate, and 1-methylhistidine.

**CONCLUSIONS:** These metabolites investigated in this study may serve as potential biomarkers of immunoglobulin A nephropathy. Point scoring of pattern recognition analysis was able to distinguish immunoglobulin A nephropathy patients from healthy controls. However, there were no obvious differences between the low-risk and high-risk groups in our research. These results offer new, sensitive and specific, noninvasive approaches that may be of great benefit to immunoglobulin A nephropathy patients by enabling earlier diagnosis.

**KEYWORDS:** Immunoglobulin A Nephropathy; Metabonomics; Biomarkers; Proton Nuclear Magnetic Resonance Spectroscopy; Orthogonal Partial Least-Squares Discriminant Analysis.

Sui W, Li L, Che W, Zuo G, Chen J, Li W, Dai Y. A proton nuclear magnetic resonance-based metabonomics study of metabolic profiling in immunoglobulin a nephropathy. *Clinics*. 2012;67(4):363-373.

Received for publication on November 28, 2011; First review completed on November 28, 2011; Accepted for publication on December 26, 2011

E-mail: [suiwg@163.com](mailto:suiwg@163.com)

Tel.: 86 0755-25626750

## INTRODUCTION

Immunoglobulin A nephropathy (IgAN) is the most common primary glomerulopathy worldwide; it is a mesangial proliferative glomerulonephritis characterized by diffuse mesangial deposition of immunoglobulin A (1).

The underlying mechanism of IgAN is poorly understood, and the outcomes of patients vary greatly. Variations in the methods used to treat IgAN patients account for less than half of the variability in outcomes (2). Determining an accurate diagnosis poses great challenges. Multiple observational cohort studies have identified several risk factors associated with the progression of IgAN (3,4). Five clinical features, namely high proteinuria, hypertension, impaired renal function, hypoproteinemia, and hyperuricemia, are independent predictors of an unfavorable renal outcome (5). However, the threshold above which the risk develops is still debated. IgAN presents with variable clinical symptoms and pathological patterns, making it difficult to predict the risk of

**Copyright** © 2012 CLINICS – This is an Open Access article distributed under the terms of the Creative Commons Attribution Non-Commercial License (<http://creativecommons.org/licenses/by-nc/3.0/>) which permits unrestricted non-commercial use, distribution, and reproduction in any medium, provided the original work is properly cited.

No potential conflict of interest was reported.

progression to end-stage renal failure in individuals. Despite the fact that the progression of IgAN is generally slow, up to 15-40% of patients with IgAN develop end-stage renal disease within 20 years (6). As a "gold standard," renal biopsy is currently the primary diagnostic tool for renal disease, as well as for treatment and prognosis. Therefore, renal biopsy has been quite helpful in the understanding of the different types of human renal diseases and has also provided insight into their pathogenesis (7). Nevertheless, renal biopsy requires an inconvenient, invasive, and painful examination that is lacking in sensitivity, specificity and reproducibility and that suffers from inappropriate categorization and can even result in some complications (4,8). Additionally, general physicians find it difficult to perform biopsies. Thus, although both the clinical and histologic features of IgAN are highly variable (9), a novel and convenient strategy for predicting diagnosis from a biopsy-based pathological evaluation has not been well established (4). Neither a biomarker nor a biomarker profile is generally accepted in clinical practice. Therefore, identifying definite, as well as sensitive, biomarkers for early diagnosis would be of great significance for making diagnostic and treatment decisions.

Metabonomics is a well-established field in systems biology, which refers to the study of individual metabolic profiles and to their changes over time due to disease, toxicity and nutritional, environmental, and genetic alterations (10-12). In a process that is known as "metabolic fingerprinting," global metabolite profiles of complex samples are used to identify potential biomarkers, and this process can provide new and unexpected insights into biological processes (13). Nuclear magnetic resonance (NMR) spectroscopy appears to be a cost-effective, useful technique for providing routine care and screening (14) and is well suited for the analysis of different types of biological fluids for the evaluation of individual metabolomes (15). Thus, proton-NMR (<sup>1</sup>H-NMR) spectroscopic analysis allows for the simultaneous detection, identification, and quantification of hundreds of low-molecular-weight metabolites (max. 20 kDa) within a biological matrix (16) for the detection of dynamic changes in global metabolism and, specifically, of noninvasive blood markers, which represents a novel and robust method for assessing organ response to pathophysiologic stimuli (17-18). Due to its usefulness in evaluating systemic responses to any subtle metabolic perturbation, <sup>1</sup>H NMR-based metabonomics has been extensively applied for the diagnosis and evaluation of cancer (19-21), diabetes (22), neurological diseases (23), heart disease (17), and cerebral infarction (24). To date, no NMR-based metabolomic studies of IgAN have been reported.

In the present work, we investigated the perturbed metabolic pattern in serum derived from IgAN patients and identified potential biomarkers of this disease using high-resolution NMR spectroscopy coupled with multivariate statistical analysis. The integration of metabolic data could provide a systematic approach for the study of metabolic profiles associated with IgAN and could facilitate a detailed examination of the underlying molecular mechanisms of the disease. We sought to determine whether we could identify the metabolic phenotypes and characterize the metabolic changes related to the degree of IgAN, whether we could distinguish valuable biomarkers for disease diagnosis, and most importantly, whether understanding the pathogenetic process of IgAN on a systemic, metabolic level could hold the key to designing

therapies to arrest the development of IgAN and prevent its later manifestations. The results highlight the possibility for "metabolic fingerprinting" to become a new diagnostic method with improved sensitivity and specificity.

## MATERIALS AND METHODS

### Subjects

Before starting this study, the patients and controls were informed of the study protocol and signed written consent forms, which were approved by the Regional Ethics Committee of the 181st Hospital Guilin, Guangxi.

For this study, 35 IgAN patients and 23 age- and sex-matched healthy controls were recruited from the Nephrology Department of the 181st Hospital Guilin, Guangxi, China, from August 2010 to December 2010. All patients with biopsy-proven primary IgAN were reviewed. The subjects were classified into three groups: a control group consisting of 23 healthy subjects, a low-risk group consisting of twenty-three IgAN patients with diseases of grades I-III based on renal biopsies stained for IgAN-A, and a high-risk group composed of twelve IgAN patients with diseases of grades IV-V based on biopsies stained for IgAN-B. The inclusion criteria for IgAN were (1) patient age ranging from 18 to 60 years and evidence of predominant mesangial IgA deposits from a renal biopsy, and (2) absence of corticosteroid or immunosuppressive therapy in the previous 10 weeks in both the patients and controls. The exclusion criteria were (1) presence of a secondary cause of IgAN, such as systemic lupus erythematosus, Schönlein-Henoch purpura, chronic liver disease, malignancies, active peptic-ulcer disease and other autoimmune disorders; (2) diagnosis of diabetes mellitus, acute interstitial nephritis, Alport's syndrome, acute myocardial infarction or stroke; (3) evidence or suspicion of severe uncontrolled hypertension (systolic blood pressure  $\geq 220$  mmHg and/or diastolic blood pressure  $\geq 120$  mmHg); and (4) history of alcoholism, smoking or oral contraception within the previous six months.

Approximately 4 mL of peripheral venous blood was collected in separate biochemistry tubes from the IgAN patients and healthy volunteers in the morning following a 12-h fasting period. The blood was allowed to clot for 60 min at room temperature and was centrifuged at 2000 $\times$ g for 10 min. The supernatants were then divided into 0.5-mL polyethylene tubes and were stored at  $-80^{\circ}\text{C}$  until the NMR analysis was performed.

### Clinical chemistry and histopathology

Clinical chemistry analyses of serum samples were conducted, using an automatic chemistry analyzer (MOL-300, Heal Force, China) with enzymatic methods using commercially available kits, for the measurement of several serum parameters, including proteinuria, alanine aminotransferase, aspartate aminotransferase, total protein, albumin, globulin, glucose, urea nitrogen, creatinine, uric acid, cholesterol, triglyceride, HDL cholesterol, and LDL cholesterol. The values were expressed as the means  $\pm$  SDs. Statistical comparisons were performed using SPSS 11.5 software (SPSS Inc., Chicago, IL, USA), and differences were considered significant when  $p < 0.05$ .

Renal tissue was obtained from all patients by percutaneous renal biopsy. Histopathological changes in kidney tissue were assessed in at least 20 randomly selected tissue sections from each group under study. Sections of 2-3  $\mu\text{m}$  in

thickness were paraffin-embedded and stained with Mayer's hematoxylin and eosin for direct immunofluorescence observations. The pathological diagnosis of IgAN was made according to the previous World Health Organization diagnostic system and its reference standard of clinical type based on Lee's classification scheme (45).

### Proton nuclear magnetic resonance spectroscopy

For the NMR experiments, the serum samples were thawed at room temperature and centrifuged at 3000×g for 5 minutes at 4°C. The supernatants were then adjusted to pH 7.4 with sodium phosphate buffer solutions and mixed with 100 µL of deuterium oxide solution to calibrate the NMR spectrometer. Finally, an aliquot of the prepared mixture (500 µL) was transferred to a 5-mm NMR tube (Wilmad, Buena, NJ, USA).

The <sup>1</sup>H NMR spectra were acquired using a Varian Unity INOVA-600 MHz NMR spectrometer (Varian Inc., Palo Alto, CA, USA) operating at a 599.93-MHz frequency and a temperature of 300 K. The spectra were acquired using a conventional presaturation pulse sequence with a NOESYPR 1-D solvent suppressor (RD-90°-t<sub>1</sub>-90°-t<sub>m</sub>-90°-ACQ). Standard two-dimensional (2-D) total correlation spectroscopy (TOCSY) NMR spectra were also acquired for spectral assignment purposes in the selected samples. <sup>1</sup>H-<sup>1</sup>H TOCSY experiments were performed using the *intocsy* pulse sequence. For each sample, the free-induction decays were collected with 128 transients into 32K data points using a spectral width of 8000 Hz with a relaxation delay of 2.1 s, an acquisition time of 1 s and a mixing time of 100 ms. All of the spectra were multiplied by an exponential weighting function corresponding to a line-broadening of 1.0 Hz prior to Fourier transformation (25).

### Data reduction and multivariate pattern recognition analysis

All of the NMR spectra were phased, baseline-corrected, and data-reduced to 225 integrated regions of δ0.002 in width, corresponding to the region of δ0.5 to δ9.0, using TopSpin software (Varian 3.0, Bruker Biospin, Germany). The <sup>1</sup>H-NMR spectra of the serum samples were referenced to the internal lactic acid CH<sub>3</sub> resonance at 1.33 ppm. Then, the region of water resonance (δ4.37-6.88) was excluded to eliminate the baseline effects of an imperfect water signal. The remaining bins were integrated and normalized for use in further analysis. The normalized data were imported into the SIMCA-P software package, version 11.0 (Umetrics AB, Umea, Sweden).

Unsupervised principal components analysis (PCA), supervised projection to partial least squares-discriminant analysis (PLS-DA), and orthogonal partial least squares-discriminant analysis (OPLS-DA) were performed for class discrimination and biomarker identification. First, PCA, based on a mean center-scaling model, was performed to examine the intrinsic variation in the dataset. The data were visualized with the score plots of the first two principal components (PC1 and PC2) to provide the most efficient two-dimensional representation of the information (21). As an extension of PLS-DA and featuring integrated orthogonal signal correction (OSC), OPLS-DA can remove variability not relevant to class separation. OPLS-DA was used to maximize the covariance between the measured data (X variable, peak intensities in NMR spectra) and the response variable (Y variable, predictive classifications) (21) and to

simultaneously remove uncorrelated variations between the X and Y variables or X variables that were orthogonal to Y variables (26). A scores plot combining the reliability and correlation from the OPLS-DA model helped to identify differential metabolites among the groups (27). The relevant metabolites for each separation model and their differences among the groups are shown as coefficient of variation plots. With a significance level of 0.05, a correlation coefficient (Corr(t,X)) of ±0.497 was adopted as a cutoff value to select the variables that were most correlated with the OPLS-DA discriminant scores. The correlation coefficients were calculated using Pearson linear correlation coefficients incorporated into MATLAB R2007a software (MathWorks, Inc., Natick, MA, USA).

Both the PLS-DA and OPLS-DA models were based on a unit variance scaling strategy. A 10-fold cross-validation was employed to obtain Q<sup>2</sup> and R<sup>2</sup> values. R<sup>2</sup> is defined as the proportion of variance in the data explained by the models and indicates goodness of fit, while Q<sup>2</sup> is defined as the proportion of variance in the data predictable by the model and indicates predictability (24). To further validate the quality of the PLS-DA model and to investigate the predictability of the OPLS-DA model, permutation tests, consisting of random permutation class membership and the performance of 200 iterations, were conducted (28). These tests compared the goodness of fit of the original model with the goodness of fit of several models based on data in which the order of the Y observations were randomly permuted while the X matrix was kept intact (29). *p*-values were generated by an unpaired *t*-test, and a *p*-value of <0.05 was considered statistically significant.

## RESULTS

### Clinical chemistry analysis and histopathology

The percentages of IgAN patients with microscopic hematuria, hypertension, hyperlipidemia, and chronic renal failure were 97.01, 27.74, 13.26, and 20.32%, respectively. A total of 80.44% of long-term hypertension patients (blood pressure >140/90 mmHg) were required to undergo anti-hypertensive therapy to maintain normotension before undergoing renal biopsy. The demographic features and body fluid parameters determined by biochemical analyses of all of the patients and healthy volunteers are shown in Table 1. No significant differences in age, sex distribution, BMI, or systolic and diastolic blood pressures were found among the three groups. The serum levels of total protein, albumin and globulin were lower in the IgAN patients than in the healthy controls, whereas the urea nitrogen, creatinine, and uric acid levels were higher in IgAN patients than in the healthy controls. Furthermore, proteinuria was significantly higher in the IgAN-B patients compared with the IgAN-A patients.

In the renal biopsy, both the IgAN-A and IgAN-B groups were similar with regard to mesangial proliferation, cellular crescents, global and segmental glomerulosclerosis, interstitial fibrosis and tubular atrophy, with some IgAN-B patients displaying a predominance of active/proliferative lesions and chronic/sclerosing lesions. As shown in Table 2, the most common IgAN pathological category in 35 cases was the mesangial proliferative type (35 cases; 57.14%), and the second most common was focal segmental glomerulosclerosis (FSGS) (12 cases; 34.29%). Membranous glomerulonephritis (MGN) (2 cases; 5.71%) and sclerosis glomerulonephritis (SGN) (1 case; 2.86%) were the next

**Table 1 - Demographic and clinical patient characteristics.**

	IgAN-A	IgAN-B	Controls
Number of samples	23	12	23
Age (years) <sup>a</sup>	31.46±9.31	36.00±7.34	35.61±11.35
Age range (years)	21-47	22-47	21-51
Sex (F/M) <sup>1</sup>	10/13	6/6	12/11
BMI (kg/m <sup>2</sup> ) <sup>a</sup>	22.35±2.22	24.60±2.41	23.40±3.26
DBP (mmHg) <sup>a</sup>	76.76±9.05	79.42±9.32	74.4±4.81
SBP (mmHg) <sup>a</sup>	125.82±12.94	126.88±16.28	125.30±11.31
Proteinuria (g/day) <sup>b</sup>	0.95±0.39	2.13±1.44	0.04±0.04
Alanine aminotransferase (U/L) <sup>a</sup>	21.28±19.32	22.71±21.59	17.48±11.96
Aspartate aminotransferase (U/L) <sup>a</sup>	23.63±12.44	23.84±11.39	18.13±11.30
Total protein (g/L) <sup>c</sup>	61.36±12.26	59.63±8.84	70.83±7.82
Albumin (g/L) <sup>b</sup>	37.06±8.00	32.94±11.65	44.43±6.34
Globulin (g/L) <sup>c</sup>	24.29±7.29	23.28±8.53	25.73±4.19
Fasting glucose (mmol/L) <sup>a</sup>	4.82±0.70	5.04±0.51	4.92±0.38
Urea nitrogen (mmol/L) <sup>b</sup>	6.04±5.36	7.29±6.30	4.56±1.13
Creatinine (µmol/L) <sup>b</sup>	109.71±49.27	123.73±47.09	87.42±13.46
Uric acid (µmol/L) <sup>b</sup>	369.56±80.76	427.84±90.39	230.16±113.76
Total cholesterol (mmol/L) <sup>a</sup>	5.61±2.07	4.62±1.26	4.53±0.84
Triglycerides (mmol/L) <sup>a</sup>	1.65±0.83	1.45±0.77	1.14±0.31
HDL cholesterol (mmol/L) <sup>c</sup>	1.68±0.61	1.75±0.42	1.43±0.53
LDL cholesterol (mmol/L) <sup>c</sup>	2.62±2.02	2.61±1.95	2.26±0.56

Data are presented as the means ± SDs.

<sup>1</sup>Categorical variables are expressed in percentages.

<sup>a</sup>There was no significant difference in demographic data among the IgAN-A, IgAN-B and control groups ( $p>0.05$ ).

<sup>b</sup>Significantly higher between the IgAN and control groups, as well as between the IgAN-A and IgAN-B groups ( $p<0.001$ ).

<sup>c</sup>Significantly lower between the IgAN and control groups, as well as between the IgAN-A and IgAN-B groups ( $p<0.05$ ).

most common disease types. The classes of the IgAN pathological grades were predominantly II, III, and IV, while grades I and V were rare. This result may have occurred because grade I corresponded to the earliest stage of kidney disease and was hidden in the clinic due to untimely treatment or insufficient medical attention, and grade V was the most severe stage of renal disease that always progressed to renal failure, often requiring dialysis treatment in the clinic. Therefore, these patients rarely underwent biopsy.

**Qualitative proton nuclear magnetic resonance analysis of serum samples**

Figure 1 depicts the typical <sup>1</sup>H CPMG spectra of serum samples obtained from healthy individuals and from IgAN-A and IgAN-B patients. The <sup>1</sup>H-NMR signals of all common metabolites, including amino acids, organic acids, and carbohydrates, were assigned according to previous publications (30). The spectral profiles were generally similar, making accurate visual comparison difficult, but some relative intensity differences could be observed among the three groups. As shown in Figure 1, predominantly

endogenous compounds were identified from the spectra comprising numerous lipoprotein fractions, some of which were derived from the glycerol of lipids, glycerolphosphocholine, low-density lipoprotein (L), and very low-density lipoprotein (VLDL). The sharp peaks arose from sugar signals, including n-acetyl glycoprotein, α-glucose, and β-glucose. There were also a large number of amino acid signals, such as methylhistidine, alanine, glutamine, glutamate, glycine, isoleucine, leucine, lysine, phenylalanine, tyrosine, and valine, as well as signals from acetate, citrate, creatine, lactate, phosphocholine, pyruvate, acetone, creatinine, myo-Inositol, and methylamine.

**Metabonomic analysis of human serum in controls and IgAN patients**

Unsupervised PCA was applied to examine the intrinsic variation in the serum data sets. Figure 2 shows the two-dimensional PCA scores plots based on the <sup>1</sup>H CPMG NMR spectra of the serum obtained from different groups. More samples were present in the 95% confidence interval of the modeled variation. We found that the control samples were very homogeneous and that their distributions of PCA score plots were relatively close. The IgAN patients and healthy controls, although scattered, were located in different clusters, demonstrating a relatively clear distinction, while the score plots showed slight separations between the IgAN-A and IgAN-B groups and the serum ( $R^2X=79.5\%$ ;  $Q^2Y=0.760$ ) models.

PLS-DA, which is more focused on detecting variation than the PCA approach, was further performed to investigate subtle metabolic differences among the groups. The parameters used to assess modeling quality, including  $R^2X$ ,  $R^2Y$ , and  $Q^2Y$ , are displayed under each picture in Figure 3. The model parameters for the explained variation,  $R^2$ , and the predictive capability,  $Q^2$ , were significantly higher ( $R^2, Q^2>0.5$ ) in the serum, indicating excellent models.

**Table 2 - Brief summary of histologic changes in 35 cases of IgAN according to Lee's classification system.**

Pathology category		I	II	III	IV	V
Mesangial proliferative	Slight	3	6	1	0	0
	Moderate	0	4	2	2	0
	Severe	0	0	1	1	0
FSGS		0	0	6	4	2
MGN		0	0	0	2	0
SGN		0	0	0	0	1
Total		3	10	10	9	3

The comparisons between all pathological types resulted in significance levels of  $p<0.01$ .





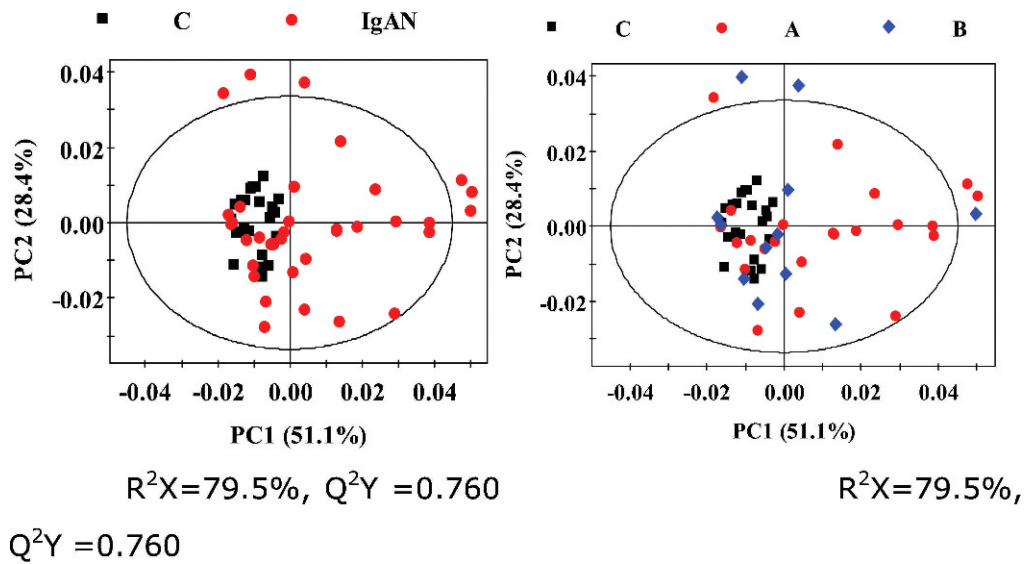


**Figure 2** - PCA scores plotted based on <sup>1</sup>H CPMG NMR spectra of serum obtained from the different groups. Left panel: C: control group, black box (■); IgAN group, red dot (●). Right panel: C: control group, black box (■); A: IgAN-A group, red dot (●); B: IgAN-B group, blue diamond (◆).

high-risk group using OPLS-DA score plots (Figure 4d, middle and right panels).

External validation was performed to test the reliability of the PLS-DA model. For our applications, the sensitivity, specificity and classification rate of the established models in correctly assigning diagnostic groups are shown in Table 3.

To further investigate the significance of these metabolites, a combination of statistical approaches was necessary (33). Thus, according to the cutoff value of the correlation coefficient, a total of 24 variables proposed as candidate biomarkers, contributing to the determination of the metabolic profiles for each model, are summarized in Table 4, along with the relative concentrations of the metabolites in the various groups.

## DISCUSSION

IgAN is a complex trait and a significant cause of renal insufficiency in different cohort populations. Many researchers have elucidated the causal mechanisms underlying IgAN in various fields. Nakamaki et al. (33) suggested that endothelin-1 is a major disease-promoting factor in renal disease. It has been documented that the deposition of polymeric IgA triggers glomerular immuno-inflammatory injury and that subsequent proteinuria may further induce tubulointerstitial lesions, thereby contributing to the progression of IgA nephropathy (34). Suzuki et al. (35) described the characteristics of IgG autoantibodies in the abnormally glycosylated IgA1 secreted by immortalized B cells derived from patients with sporadic forms of IgA nephropathy, which may offer new insights into disease pathogenesis and may lead to new methods of diagnosis, monitoring, and therapy for patients with IgA nephropathy. Many IgAN studies have been published, but most have suffered from small sample sizes and methodological problems, and none of the results have been convincingly validated. Therefore, the molecular basis of IgA nephropathy is still not fully understood.

In our study, NMR-based metabolomic analysis technology was used for the first time to identify the characteristics of metabolite profiles from the serum samples of IgAN patients and from age- and sex-matched healthy controls. Using a comprehensive NMR screening process, we aimed to assess the potential of the technique as a diagnostic tool for the disease and to identify the characteristics of metabolites. The discovery of distinctive patterns in the metabolite profiles associated with different renal conditions could be of great diagnostic significance. The PCA score plots achieved good separation between the IgAN patients and healthy controls, and the IgAN-A and IgAN-B samples manifested similar global differences in metabolic profiles. The results support the hypothesis that the metabolic fingerprinting of serum could be useful in distinguishing IgAN patients from healthy individuals. Upon testing of these results, the OPLS-DA models showed considerable  $R^2$  and  $Q^2$  values. Importantly, the results showed high sensitivity and specificity for diagnosing patients with IgAN. However, this technique was not sensitive enough to differentiate between high and low disease risk. This finding suggests that the diseases may share, to some extent, the same metabolic pathway in their pathogenesis. Nevertheless, potential biomarkers, including  $\beta$ -glucose,  $\alpha$ -glucose, valine, tyrosine, pyruvate, phenylalanine, phosphocholine, *myo*-Inositol, lysine, lactate, L6 lipids (=CH-CH<sub>2</sub>-CH=), L5 lipids (-CH<sub>2</sub>-C=O), L3 lipids (-CH<sub>2</sub>-CH<sub>2</sub>-C=O), isoleucine, glycerolphosphocholine, glycine, glutamine, glutamate, creatinine, creatine alanine, acetate, 3-hydroxybutyrate and 1-methylhistidine, as detected in this study, might explain the pathogenesis of IgAN and warrant further investigation in a systemic review.

Similar to how genes and proteins are normally associated with specific pathways and processes, so are metabolites. Changes in the relative concentrations of certain "universal" metabolites, such as glucose, lactate, and citrate, reflect changes in cell viability (apoptosis), levels of oxygenation (anoxia, ischemia, and oxidative stress), local pH, and general homeostasis (36). Among these metabolites,

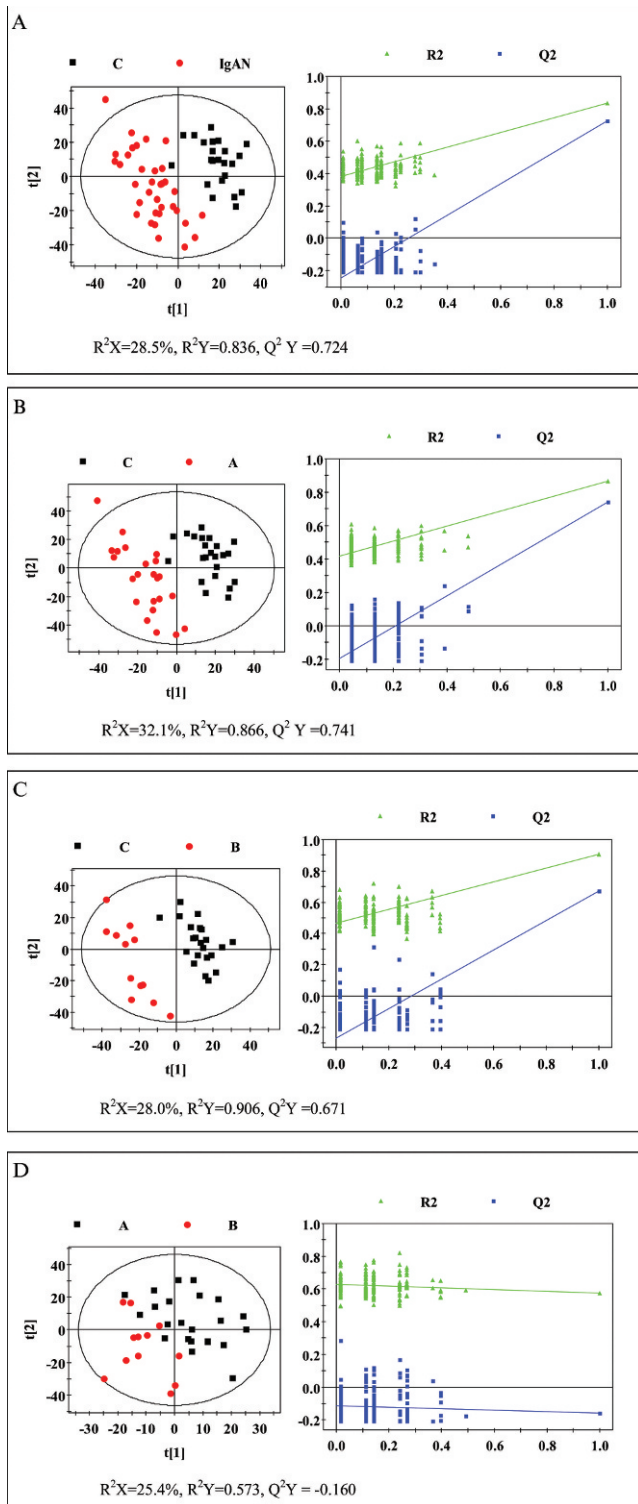


**Figure 3** - Cross-validation of partial least squares-discriminant analysis (PLS-DA) models obtained from 200 permutation tests. PLS-DA score plots showing the separation between (a) controls and IgAN patients, (b) controls and IgAN-A patients, (c) controls and IgAN-B patients, and (d) IgAN-A and IgAN-B patients.

we observed significantly elevated levels of lactate and pyruvate in the serum of IgAN-A patients, while neither could be detected in IgAN-B patients. Graham et al. (37) suggested that lactate arises from a shift toward anaerobic

glycolysis in potentially viable cells that continue to metabolize glucose under local hypoxic conditions. Alternatively, high levels of lactate may arise from inflammatory and phagocytic cell infiltration in tissue. Additionally, these are types of energy metabolism processes, especially anaerobic glycolysis. Because an increase in anaerobic cell respiration occurs under renal damage, there is an increased concentration of lactate and pyruvate in IgAN-A serum due to anaerobic glycolysis of serum glucose. In combination with a lower level of glucose, this result indicates up-regulated glycolysis. Furthermore, possibly due to the reduced utilization of pyruvate in the Krebs cycle, citrate levels also decrease. Glucose and pyruvate can obviously be quite informative with regard to cell function or cell stress and, therefore, organ function.

IgAN causes perturbations in the Krebs cycle, as well as increased protein degradation from cell necrosis, leading to altered concentrations of free amino acids in serum. In this study, the significantly decreased amounts of valine, tyrosine, lysine, isoleucine, glycine, glutamate, and alanine may be associated with reduced translation from citrate,  $\alpha$ -ketoglutarate, succinyl-CoA and fumarate, which are intermediates of the Krebs cycle. Such results may indicate that protein is degraded into amino acids to regulate biological functions, such as gene transcription, cell cycle progression, and inflammatory and autoimmunity responses. The results are also indicative of alterations in energy metabolism as well as impairment in mitochondrial function (38). This finding is consistent with our report (Table 1) of decreased levels of total protein, albumin, and globulin in serum clinical chemistry assays. The lower level of glutamine may result from the inadequacy of  $\alpha$ -ketoglutarate, which fluxes out of the mitochondria and is converted into glutamate in the cytosol.

Other types of metabolites are specifically associated with tissue remodeling, muscle atrophy and myofibrillar breakdown (e.g., methylhistidine, creatine, creatinine, and glycine). Changes in the levels of these metabolites can provide important information regarding the extent of tissue repair or tissue damage (39,40). Thus, an elevation in creatine/creatinine levels is indicative of damage to the renal parenchyma or of kidney necrosis, which is also in accordance with clinical chemistry assays. Moreover, the lower concentrations of 1-methylhistidine, which is metabolized into histidine, might be closely related to protein energy wasting, inflammation and oxidative stress (41).

Phosphorylcholine is a precursor of glycerolphosphorylcholine, which is an essential component of membrane structures. The decreased serum levels of phosphorylcholine in both the IgAN-A and IgAN-B patients might be related to the augmented utilization of glycerolphosphorylcholine in impaired cells and organelle membranes. More recent evidence has demonstrated that the proportion of PC/GPC can be used as a measurement of enhanced cell proliferation in cancerous tissues (42).

*Myo*-Inositol, L6 lipids (=CH-CH<sub>2</sub>-CH=), L5 lipids (-CH<sub>2</sub>-C=O), and L3 lipids (-CH<sub>2</sub>-CH<sub>2</sub>-C=O) are involved in lipid metabolism. In our study, clinical chemistry assays indicated slightly higher levels of free fatty acids and no significant differences in levels of triglycerides or total cholesterol between the IgAN and control groups, as well as between the IgAN-A and IgAN-B groups. NMR spectra showed enhanced serum levels of VLDL/LDL and unsaturated lipids in the IgAN patients. The enhanced lipid levels



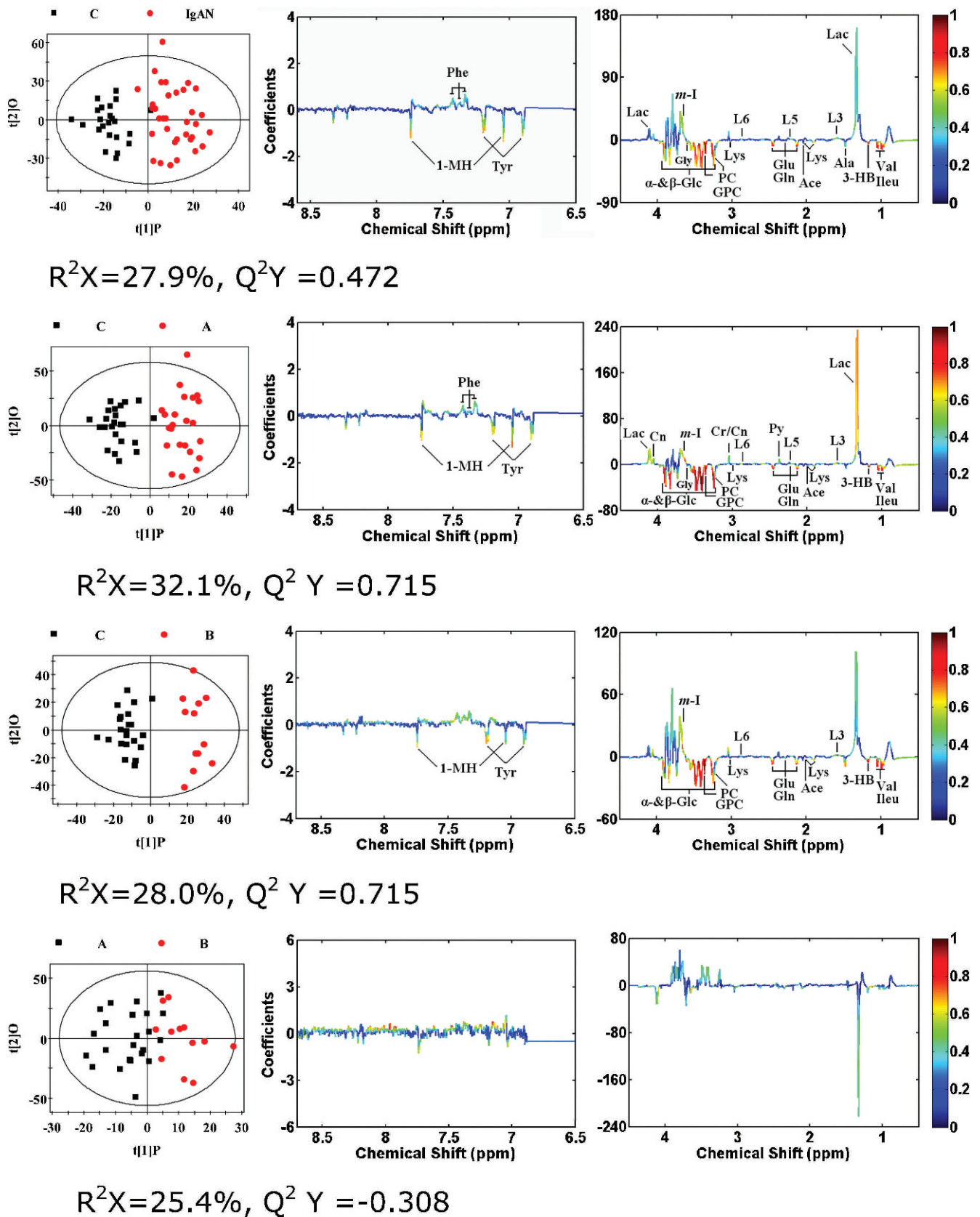


Figure 4 - OPLS-DA score plots (left panel) derived from <sup>1</sup>H NMR spectra of serum and corresponding coefficient loading plots (middle and right panels) obtained from different groups. Keys for the assignments are shown in Figure 1.



**Table 3** - Sensitivity, specificity and classification rate calculated for the cross-validated OPLS-DA model applied to the spectra of serum samples from healthy controls and patients with IgAN.

	IgAN vs. control	IgAN-A vs. control	IgAN-B vs. control	IgAN-A vs. IgAN-B
Sensitivity (%)	88.6	92.3	95.4	-
Specificity (%)	97.1	100	100	-
Classification rate (%)	93.1	97.0	98.2	-

can most likely be attributed to the lower activity of the lipoprotein lipase. Additionally, the increase in lipid metabolism is enhanced in response to kidney injury when IgAN occurs (21). The increase in acetate, which is the end product of lipid metabolism, further supports the above-mentioned hypothesis. Furthermore, our work demonstrated that the concentrations of serum 3-hydroxybutyrate in the renal tissue of IgAN patients were significantly lower than those in the renal tissue of controls, which may confirm the shift in energy metabolism toward the formation and utilization of ketone bodies.

In summary, the systemic changes in endogenous metabolites from IgAN patients mainly influenced energy, amino acid, lipid, and nucleotide metabolism. As shown in Figure 5, the number of metabolic pathways involved in IgAN highlights the complexity of the metabolic response to IgAN. Metabolite profiling, obtained from <sup>1</sup>H-NMR-based metabonomic analysis of IgAN serum samples, clearly distinguished IgAN patients from healthy controls, which may be a minimally invasive method for detecting IgAN before symptoms develop, suggesting that the utilization of

metabonomics in serum may assist in early diagnosis, more appropriate therapy and better clinical management.

Although we identified disease-specific metabolite profiles, the future use of metabolite biomarkers in the clinical environment requires optimization to improve their accuracy. The limitations of this study must also be recognized (43,44). First, metabolic investigations can be helpful for the differentiation of healthy controls from IgAN patients, but they are not sensitive enough to be used to draw conclusions about the dynamic processes of high and low risk for this disease. Moreover, different histological classifications subjectively present selection bias to a certain degree when screening patients. Histological classification must be validated in different cohorts. Furthermore, this study was not specifically designed to answer the question of whether medical treatment consisting of diuretics, angiotensin-converting enzyme inhibitors and/or angiotensin II receptor blockers, n-3 polyunsaturated fatty acids, and hypolipidemic agents should be administered to IgAN patients. We did not evaluate the associations between therapeutic interventions and metabolite changes in this

**Table 4** - Summary of the <sup>1</sup>H NMR-detected statistically significant changes in the relative levels of serum metabolites for IgAN patients compared with the healthy controls.

Metabolites	r <sup>a</sup>			
	C-IgAN	C- A	C- B	A-B
β-Glucose: 3.25 (dd <sup>b</sup> ), 3.41 (t), 3.46 (m), 3.49 (t), 3.90 (dd), 4.65 (d)	-0.784	-0.859	-0.797	-
α-Glucose: 3.42 (t), 3.54 (dd), 3.71 (t), 3.73 (m), 3.84 (m), 5.23 (d)	-0.812	-0.843	-0.871	-
Valine: 0.99 (d), 1.04 (d)	-0.816	-0.799	-0.811	-
Tyrosine: 6.89 (d), 7.19 (d)	-0.619	-0.638	-0.652	-
Pyruvate: 2.37 (s)	-	0.426	-	-
Phenylalanine: 7.32 (d), 7.37 (t), 7.42 (dd)	0.436	0.473	-	-
Phosphocholine: 3.21 (s), 3.35 (s)	-0.791	-0.747	-0.798	-
myo-Inositol: 3.65 (dd)	0.513	0.671	0.672	-
Lysine: 1.72 (m), 1.90 (m), 3.02 (t), 3.76 (m)	-0.577	-0.546	-0.560	-
Lactate: 1.33 (d), 4.11 (q)	0.445	0.611	-	-
L6 lipid, =CH-CH <sub>2</sub> -CH=: 2.78 (br)	0.422	0.555	0.617	-
L5 lipid, -CH <sub>2</sub> -C=O: 2.24 (br)	0.433	0.514	-	-
L3 lipid, -CH <sub>2</sub> -CH <sub>2</sub> -C=O: 1.58 (br)	0.527	0.610	0.561	-
Isoleucine: 0.94 (t), 1.01 (d)	-0.650	-0.604	-0.644	-
Glycerolphosphocholine: 3.22 (s), 3.36 (s)	-0.876	-0.858	-0.878	-
Glycine: 3.56 (s)	-0.524	-0.477	-	-
Glutamine: 2.14 (m), 2.45 (m), 3.78 (t)	-0.762	-0.796	-0.707	-
Glutamate: 2.10 (m), 2.35 (m), 3.78 (t)	-0.762	-0.751	-0.697	-
Creatinine: 3.04 (s), 4.06 (s)	-	0.506	-	-
Creatine: 3.04 (s), 3.93 (s)	-	0.417	-	-
Alanine: 1.48 (d)	-0.451	-	-	-
Acetate: 1.92 (s)	-0.519	-0.454	-0.563	-
3-Hydroxybutyrate: 1.18 (d)	-0.834	-0.823	-0.843	-
1-Methylhistidine: 7.05 (s), 7.75 (s)	-0.692	-0.674	-0.608	-

OPLS-DA coefficients derived from the NMR data of metabolites in serum obtained from different groups.

<sup>a</sup>Correlation coefficients and positive and negative signs indicate positive and negative correlations in the concentrations, respectively. The correlation coefficient of  $|r| > 0.404$  was used as the cutoff value for statistical significance based on the discrimination significance at the level of  $p = 0.05$  and  $df$  (degree of freedom) = 22 (for C-IgAN and C-A), and it was  $|r| > 0.553$  at the level of  $p = 0.05$  for  $df = 11$  (for C-B and A-B). "-" means that the correlation coefficient  $|r|$  is less than the cutoff value.

<sup>b</sup>Multiplicity: s, singlet; d, doublet; t, triplet; q, quartet; dd, doublet of doublets; m, multiplet.

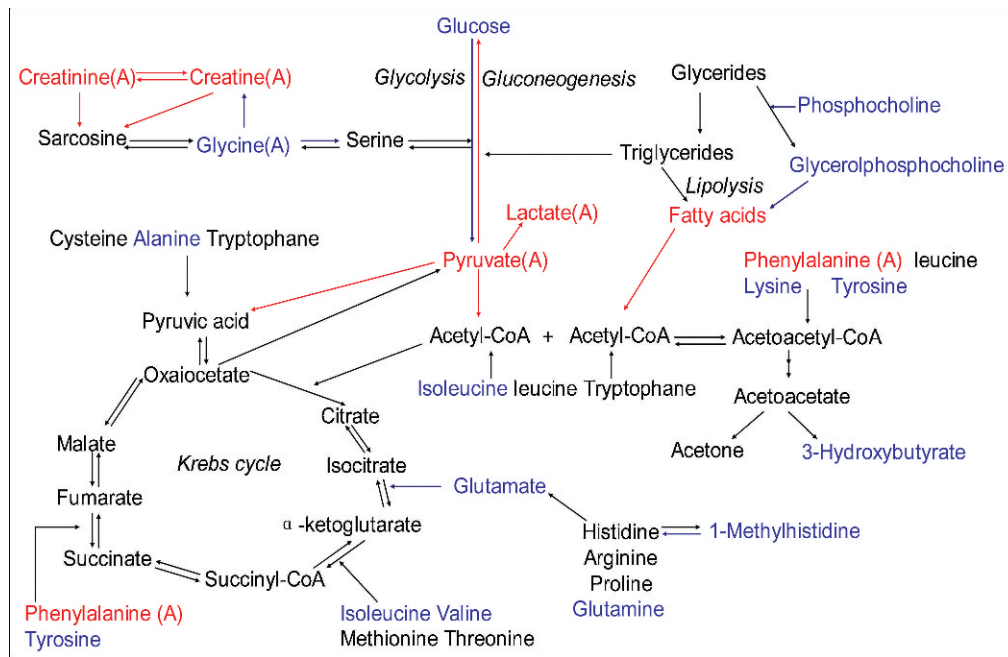


**Figure 5** - Summary of the metabolic pathways in which the metabolites described in this article are involved. Red indicates enhanced metabolite levels, blue indicates reduced metabolite levels, and black indicates metabolites not found or not identified. (A) represents the changes only found in the IgAN-A group.

cohort of patients. Finally, given our relatively small sample size, especially the IgAN-B sample size, our observations still remain to be verified in larger studies. Further studies with larger numbers of patients and controls, including other distinctive types of IgAN diseases, will be crucial to validating this model and to assuring its use in routine practice. Additionally, to explore the potential of this model, follow-up work is required, which should include long-term studies of large numbers of patients with early IgAN diagnoses. It is also necessary to validate these biomarkers in another cross-sectional study with a separate population, and it would be of interest to perform a longitudinal study to determine the predictive power of this model with regard to disease progression.

In conclusion, this study showed that one potential use of metabonomics might be the development of a more sensitive, reliable and successful method of diagnosis than the invasive puncture procedure for distinguishing IgAN patients from healthy controls. Nevertheless, the model of the high-risk IgAN group versus the low-risk group was not perfect; that is, the <sup>1</sup>H NMR-based metabonomic analysis of serum samples revealed some characteristic metabolic features, but not processes, of the pathological changes associated with IgAN. Further NMR-based metabonomic studies of various IgAN models could provide insight into the molecular mechanisms involved in the pathogenesis of IgAN and could offer invaluable information that could be used in the development of a novel diagnostic technique and better IgAN treatments.

## ACKNOWLEDGMENTS

This project was funded by grant support received from the Natural Science Foundation of Guangxi, China, which is gratefully acknowledged (fund number 2010GXNSFA013273). We are also thankful to the patients and healthy volunteers who participated in this study.

## AUTHOR CONTRIBUTIONS

Sui W collected data and wrote the paper. Li L performed the research and wrote the paper. Che Wand Chen J analyzed the data. Zuo G and Li W revised the paper. Dai Y designed the research protocol and revised the paper.

## REFERENCES

1. D'Amico G. The commonest glomerulonephritis in the world: IgA nephropathy. *Q J Med.* 1987;64(245):709-27.
2. Bartosik LP, Lajoie G, Sugar L, Catran DCPredicting progression in IgA nephropathy. *Am J Kidney Dis.* 2001;38(4):728-35, <http://dx.doi.org/10.1053/ajkd.2001.27689>.
3. Coppo R, D'Amico G. Factors predicting progression of IgA nephropathies. *J Nephrol.* 2005;18(5):503-12.
4. Yamamoto R, Imai E. A novel classification for IgA nephropathy. *Kidney International.* 2009;76(3):477-80, <http://dx.doi.org/10.1038/ki.2009.206>.
5. Le W, Liang S, Hu Y, Deng K, Bao H, Zeng C, et al. Long-term renal survival and related risk factors in patients with IgA nephropathy: results from a cohort of 1155 cases in a Chinese adult population. *Nephrol Dial Transplant.* 2011;29: [Epub ahead of print].
6. Laville M, Alamartine E. Treatment options for IgA nephropathy in adults: a proposal for evidence-based strategy. *Nephrol Dial Transplant.* 2004;19(8):1947-51, <http://dx.doi.org/10.1093/ndt/gfh309>.
7. Carvalho E, do Sameiro Faria M, Nunes JP, Sampaio S, Valbuena C. Renal diseases: a 27-year renal biopsy study. *J Nephrol.* 2006;19(4):500-7.
8. Weiguo Sui, Yong Dai, Yue Zhang, Jiejing Chen, Huaying Liu, He Huang, et al. Proteomic profiling of immunoglobulin A nephropathy in serum using magnetic bead based sample fractionation and matrix-assisted laser desorption/ionization-time of flight mass spectrometry. *Saudi Med J.* 2010;31(12):2-3.
9. Peters HP, van den Brand JA, Wetzels JF. Urinary excretion of low-molecular-weight proteins as prognostic markers in IgA nephropathy. *Neth J Med.* 2009;67(2):54-61.
10. Lindon JC, Nicholson JK. Analytical technologies for metabonomics and metabolomics, and multi-omic information recovery. *Trends Anal. Chem.* 2008;27(3):194-204, <http://dx.doi.org/10.1016/j.trac.2007.08.009>.
11. Coen M, Holmes E, Lindon JC, Nicholson JK. NMR-based metabolic profiling and metabonomic approaches to problems in molecular toxicology. *Chem Res Toxicol.* 2008;21(1):9-27, <http://dx.doi.org/10.1021/tx700335d>.
12. Holmes E, Loo RL, Stalmer J, Bictash M, Yap IK, Chan Q, et al. Human metabolic phenotype diversity and its association with diet and blood pressure. *Nature.* 2008;453(7193):396-400, <http://dx.doi.org/10.1038/nature06882>.

13. Kaddurah-Daouk R, Krishnan KR. Metabolomics: a global biochemical approach to the study of central nervous system diseases. *Neuropsychopharmacology*. 2009;34(1):173–86, <http://dx.doi.org/10.1038/npp.2008.174>.
14. Ala-Korpela M. Potential role of body fluid <sup>1</sup>H NMR metabonomics as a prognostic and diagnostic tool. *Expert Rev Mol Diagn*. 2007;7(6):761-73, <http://dx.doi.org/10.1586/14737159.7.6.761>.
15. Pradat PF, Dib M. Biomarkers in amyotrophic lateral sclerosis: facts and future horizons. *Mol Diagn Ther*. 2009;13(2):115-25.
16. Serkova N, Klawitter J, Niemann CU. Organ-specific response to inhibition of mitochondrial metabolism by cyclosporine in the rat. *Transpl Int*. 2003;16(10):748-55, <http://dx.doi.org/10.1111/j.1432-2277.2003.tb00235.x>.
17. Brindle JT, Antti H, Holmes E, Tranter G, Nicholson JK, Bethell HW, et al. Rapid and noninvasive diagnosis of the presence and severity of coronary heart disease using <sup>1</sup>H-NMR-based metabolomics. *Nat Med*. 2002;8(12):1439-44, <http://dx.doi.org/10.1038/nm1202-802>.
18. Beckwith-Hall BM, Holmes E, Lindon JC, Gounarides J, Vickers A, Shapiro M, et al. NMR-based metabolomic studies on the biochemical effects of commonly used drug carrier vehicles in the rat. *Chem Res Toxicol*. 2002;15(9):1136-41, <http://dx.doi.org/10.1021/tx020020+>.
19. Ludwig C, Ward DG, Martin A, Viant MR, Ismail T, Johnson PJ, et al. Fast targeted multidimensional NMR metabolomics of colorectal cancer. *Magn Reson Chem*. 2009;47(Suppl 1):S68-73, <http://dx.doi.org/10.1002/mrc.2519>.
20. Tiziani S, Lopes V, Günther UL. Early stage diagnosis of oral cancer using <sup>1</sup>H NMR-based metabolomics. *Neoplasia*. 2009;11(3):269-76.
21. Gao H, Lu Q, Liu X, Cong H, Zhao L, Wang H, et al. Application of <sup>1</sup>H NMR-based metabolomics in the study of metabolic profiling of human hepatocellular carcinoma and liver cirrhosis. *Cancer Sci*. 2009;100(4):782-5, <http://dx.doi.org/10.1111/j.1349-7006.2009.01086.x>.
22. Maher AD, Crockford D, Toft H, Malmodin D, Faber JH, McCarthy MI, et al. Optimization of human plasma <sup>1</sup>H NMR spectroscopic data processing for high-throughput metabolic phenotyping studies and detection of insulin resistance related to type 2 diabetes. *Anal Chem*. 2008;80(19):7354-62, <http://dx.doi.org/10.1021/ac801053g>.
23. Quinones MP, Kaddurah-Daouk R. Metabolomics tools for identifying biomarkers for neuropsychiatric diseases. *Neurobiol Dis*. 2009;35(2):165-76, <http://dx.doi.org/10.1016/j.nbd.2009.02.019>.
24. Jung JY, Lee HS, Kang DG, Kim NS, Cha MH, Bang OS, et al. <sup>1</sup>H-NMR-Based Metabolomics Study of Cerebral Infarction. *Stroke*. 2011;42(5):1282-8, <http://dx.doi.org/10.1161/STROKEAHA.110.598789>.
25. Kang SM, Park JC, Shin MJ, Lee H, Oh J, Ryu do H, et al. (1)H nuclear magnetic resonance based metabolic urinary profiling of patients with ischemic heart failure. *Clin Biochem*. 2011;44(4):293-9, <http://dx.doi.org/10.1016/j.clinbiochem.2010.11.010>.
26. Larsen FH, van den Berg F, Engelsen SB. An exploratory chemometric study of <sup>1</sup>H NMR spectra of table wines. *J Chemometr*. 2006;20(4):198-208, <http://dx.doi.org/10.1002/cem.991>.
27. Wiklund S, Johansson E, Sjöström L, Mellerowicz EJ, Edlund U, Shockcor JP, et al. Visualization of GC/TOF-MS-based metabolomics data for identification of biochemically interesting compounds using OPLS class models. *Anal Chem*. 2008;80(1):115-22, <http://dx.doi.org/10.1021/ac0713510>.
28. Ni Y, Su M, Lin J, Wang X, Qiu Y, Zhao A, et al. Metabolic profiling reveals disorder of amino acid metabolism in four brain regions from a rat model of chronic unpredictable mild stress. *FEBS Lett*. 2008;582(17):2627-36, <http://dx.doi.org/10.1016/j.febslet.2008.06.040>.
29. Aarøe J, Lindahl T, Dumeaux V, Sæbø S, Tobin D, Hagen N, et al. Gene expression profiling of peripheral blood cells for early detection of breast cancer. *Breast Cancer Res*. 2010;12(1):R7, <http://dx.doi.org/10.1186/bcr2472>.
30. Wishart DS, Lewis MJ, Morrissey JA, Flegel MD, Jeroncic K, Xiong Y, et al. The human cerebrospinal fluid metabolome. *J Chromatogr B Analyt Technol Biomed Life Sci*. 2008;871(2):164-73.
31. Kang SM, Park JC, Shin MJ, Lee H, Oh J, Ryu do H, et al. <sup>1</sup>H nuclear magnetic resonance based metabolic urinary profiling of patients with ischemic heart failure. *Clinical Biochemistry*. 2011;44(4):293-9, <http://dx.doi.org/10.1016/j.clinbiochem.2010.11.010>.
32. Grove H, Jørgensen BM, Jessen F, Søndergaard I, Jacobsen S, Hollung K, et al. Combination of statistical approaches for analysis of 2-DE data gives complementary results. *J Proteome Res*. 2008;7(12):5119-24, <http://dx.doi.org/10.1021/pr800424c>.
33. Nakamaki S, Satoh H, Kudoh A, Hayashi Y, Hirai H, Watanabe T. Adiponectin reduces proteinuria in streptozotocin-induced diabetic Wistar rats. *Exp Biol Med (Maywood)*. 2011;236(5):614-20, <http://dx.doi.org/10.1258/ebm.2011.010218>.
34. Rifai A, Dworkin LD. IgA nephropathy: markers of progression and clues to pathogenesis. *Kidney Int*. 2008;73(12):1338–40, <http://dx.doi.org/10.1038/ki.2008.158>.
35. Suzuki H, Moldoveanu Z, Hall S, Brown R, Vu HL, Novak L, et al. IgA1 secreting cell lines from patients with IgA nephropathy produce aberrantly glycosylated IgA1. *J Clin Invest*. 2008;118(2):629–39.
36. Oberholzer J, Testa G, Sankary H, et al. Kidney transplantation at the University of Illinois at Chicago from 1988–2004. *Clin Transpl*. 2004;143–9.
37. Graham GD, Blamire AM, Howseman AM, Rothman DL, Fayad PB, Brass LM, et al. Proton magnetic resonance spectroscopy of cerebral lactate and other metabolites in stroke patients. *Stroke*. 1992;23(3):333–40, <http://dx.doi.org/10.1161/01.STR.23.3.333>.
38. Waters NJ, Waterfield CJ, Farrant RD, Holmes E, Nicholson JK. Metabonomic deconvolution of embedded toxicity: application to thioacetamide hepato- and nephrotoxicity. *Chem Res Toxicol*. 2005;18(4):639-54.
39. Nicholson JK, Lindon JC, Holmes E. 'Metabonomics': understanding the metabolic responses of living systems to pathophysiological stimuli via multivariate statistical analysis of biological NMR spectroscopic data. *Xenobiotica*. 1999;29(11):1181–9, <http://dx.doi.org/10.1080/004982599238047>.
40. Lindon JC, Holmes E, Bollard ME, Stanley EG, Nicholson JK. Metabonomics technologies and their applications in physiological monitoring, drug safety assessment and disease diagnosis. *Biomarkers*. 2004;9(1):1–31, <http://dx.doi.org/10.1080/13547500410001668379>.
41. Kumar A, Bala L, Kalita J, Misra UK, Singh RL, Khetrpal CL, et al. Metabolomic analysis of serum by (1) H NMR spectroscopy in amyotrophic lateral sclerosis. *Clin Chim Acta*. 2010;411(7-8):563-7, <http://dx.doi.org/10.1016/j.cca.2010.01.016>.
42. Glunde K, Ackerstaff E, Mori N, Jacobs MA, Bhujwala ZM. Choline phospholipid metabolism in cancer: consequences for molecular pharmaceutical interventions. *Mol Pharm*. 2006;3:496-506, <http://dx.doi.org/10.1021/mp060067e>.
43. Lovejoy TI, Revenson TA, France CR. Reviewing manuscripts for peer-review journals: a primer for novice and seasoned reviewers. *Ann Behav Med*. 2011;42(1):1-13, <http://dx.doi.org/10.1007/s12160-011-9269-x>.
44. Garmel GM. Reviewing manuscripts for biomedical journals. *Perm J*. 2010;14(1):32-40.
45. Lee SM, Rao VM, Franklin WA, Schiffer MS, Aronson AJ, Spargo BH, et al. IgA nephropathy: morphologic predictors of progressive renal disease. *Hum Pathol*. 1982;13(4):314-22, [http://dx.doi.org/10.1016/S0046-8177\(82\)80221-9](http://dx.doi.org/10.1016/S0046-8177(82)80221-9).